



# MIT Open Access Articles

## *Dynamics of collapsed polymers under the simultaneous influence of elongational and shear flows*

The MIT Faculty has made this article openly available. **Please share** how this access benefits you. Your story matters.

<b>Citation</b>	Sing, Charles E., and Alfredo Alexander-Katz. Dynamics of Collapsed Polymers Under the Simultaneous Influence of Elongational and Shear Flows. The Journal of Chemical Physics 135, no. 1 (2011): 014902. © 2011 American Institute of Physics.
<b>As Published</b>	<a href="http://dx.doi.org/10.1063/1.3606392">http://dx.doi.org/10.1063/1.3606392</a>
<b>Publisher</b>	American Institute of Physics
<b>Version</b>	Final published version
<b>Accessed</b>	Wed Dec 05 22:45:14 EST 2018
<b>Citable Link</b>	<a href="http://hdl.handle.net/1721.1/79371">http://hdl.handle.net/1721.1/79371</a>
<b>Terms of Use</b>	Article is made available in accordance with the publisher's policy and may be subject to US copyright law. Please refer to the publisher's site for terms of use.
<b>Detailed Terms</b>	

## Dynamics of collapsed polymers under the simultaneous influence of elongational and shear flows

Charles E. Sing and Alfredo Alexander-Katz

Citation: *J. Chem. Phys.* **135**, 014902 (2011); doi: 10.1063/1.3606392

View online: <http://dx.doi.org/10.1063/1.3606392>

View Table of Contents: <http://jcp.aip.org/resource/1/JCPSA6/v135/i1>

Published by the AIP Publishing LLC.

### Additional information on J. Chem. Phys.

Journal Homepage: <http://jcp.aip.org/>

Journal Information: [http://jcp.aip.org/about/about\\_the\\_journal](http://jcp.aip.org/about/about_the_journal)

Top downloads: [http://jcp.aip.org/features/most\\_downloaded](http://jcp.aip.org/features/most_downloaded)

Information for Authors: <http://jcp.aip.org/authors>

## ADVERTISEMENT

**physicstoday**

Comment on any  
*Physics Today* article.

**Measured energy in Japan**  
David von Seggern  
([dvseg@seismo.unr.edu](mailto:dvseg@seismo.unr.edu)) University of Nevada  
July 2012, page 10  
DIGITAL OBJECT IDENTIFIER  
<http://dx.doi.org/10.1063/PT.3.1619>

**Comment on this article**  
By the act of hitting a ball with a bat, one calculates the force energy to deliver the ball to its new location, but one must also take into account that the ball extended its energy release to that which became struck by the ball as its momentum ceased and passed energy to the struck team. Therefore the parameters of the damage extend into the future when the received energy to that pushed upon, later becomes released in a new event. Perhaps calculations of one added that in while another's calculations did not. E.M.C.  
Written by Edgar Mocarvill, 14 July 2012 19:59

# Dynamics of collapsed polymers under the simultaneous influence of elongational and shear flows

Charles E. Sing<sup>a)</sup> and Alfredo Alexander-Katz<sup>b)</sup>

Department of Materials Science and Engineering, Massachusetts Institute of Technology,  
77 Massachusetts Ave., Cambridge, Massachusetts 02139, USA

(Received 3 May 2011; accepted 8 June 2011; published online 5 July 2011)

Collapsed polymers in solution represent an oft-overlooked area of polymer physics, however recent studies of biopolymers in the bloodstream have suggested that the physics of polymer globules are not only relevant but could potentially lead to powerful new ways to manipulate single molecules using fluid flows. In the present article, we investigate the behavior of a collapsed polymer globule under the influence of linear combinations of shear and elongational flows. We generalize the theory of globule-stretch transitions that has been developed for the specific case of simple shear and elongational flows to account for behavior in arbitrary flow fields. In particular, we find that the behavior of a globule in flow is well represented by a two-state model wherein the critical parameters are the transition probabilities to go from a collapsed to a stretched state  $P_{g-s}$  and vice versa  $P_{s-g}$ . The collapsed globule to stretch transition is described using a nucleation protrusion mechanism, and the reverse transition is described using either a tumbling or a relaxation mechanism. The magnitudes of  $P_{g-s}$  and  $P_{s-g}$  govern the state in which the polymer resides; for  $P_{g-s} \approx 0$  and  $P_{s-g} \approx 1$  the polymer is always collapsed, for  $P_{g-s} \approx 0$  and  $P_{s-g} \approx 0$  the polymer is stuck in either the collapsed or stretched state, for  $P_{g-s} \approx 1$  and  $P_{s-g} \approx 0$  the polymer is always stretched, and for  $P_{g-s} \approx 1$  and  $P_{s-g} \approx 1$  the polymer undergoes tumbling behavior. These transition probabilities are functions of the flow geometry, and we demonstrate that our theory quantitatively predicts globular polymer conformation in the case of mixed two-dimensional flows, regardless of orientation and representation, by comparing theoretical results to Brownian dynamics simulations. Generalization of the theory to arbitrary three-dimensional flows is discussed as is the incorporation of this theory into rheological equations. © 2011 American Institute of Physics. [doi:10.1063/1.3606392]

There has been significant interest in the last few decades into the interaction of polymers and fluid flows, mostly focusing on the viscosity behavior of dilute solutions of random and expanded coils under typical fluid flows. Pioneering theoretical work by DeGennes was followed up by a large body of work, both experimentally and computationally.<sup>1-5</sup> More recently, fluorescent microscopy methods have allowed single molecules of DNA to be analyzed to evaluate the accuracy of these models and experiments and to place them in the context of more easily-observable macroscopic properties.<sup>6-9</sup> Also, new applications of this fundamental physical understanding have proven valuable in the field of DNA analysis using microfluidics.<sup>10,11</sup>

Only very recently, however, has the case of collapsed coils in a fluid flow been considered.<sup>12-17</sup> For most synthetic polymer applications, this negligence is due to the very narrow window where collapsed polymers can be suspended in solution without undergoing macroscopic phase separation. However, there has been a renewed interest in collapsed polymers in recent years due to the interest in understanding the behavior of proteins such as von Willebrand Factor (vWF) that are regulated by fluid flows.<sup>15,18-20</sup> It has been shown that proteins of this type can be well described by the physics of collapsed homopolymers, and the dynamics in shear and

elongational flows have been thoroughly examined by the authors.<sup>12-16</sup> This previous work has already elucidated much of the behavior of vWF in experiment, where flow conditions are generally well behaved; however we desire to extend this work to more complicated situations that may exist *in vivo* and thus a more general theory of globule-stretch transitions is necessary.<sup>15</sup> Furthermore, as the field of single-chain manipulation matures as a field, the on-off functionality of a globule-stretch transition may be an attractive avenue for conformational control of synthetic polymers that have been kinetically stabilized against aggregation.

In the present article, we investigate the implication of flows that do not have purely elongational or shear character, but instead have a linear combination of the two flow profiles. This will provide a more thorough understanding of the behavior of proteins in more complex flow profiles, which tend to lie somewhere in the continuum between the two extremes of elongational and shear flow.

## I. SIMULATION METHODS

The polymer is modeled as a chain of  $N$  beads of radius  $a$ , interacting through a potential  $U$  given by

$$\frac{U}{k_B T} = \frac{\kappa}{2} \sum_{i=1}^{N-1} (r_{i+1,i} - 2a)^2 + \tilde{u} \sum_{ij} ((2a/r_{i,j})^{12} - 2(2a/r_{i,j})^6), \quad (1)$$

<sup>a)</sup>Electronic mail: cesing@mit.edu.

<sup>b)</sup>Electronic mail: aalexander@mit.edu.

where  $r_{i,j}$  is the distance between beads  $i$  and  $j$ . The first term accounts for the connectivity of the chain, with the bead-bead spring constant  $\kappa$  chosen to be  $> 100/a^2$  such that there are negligible deviations of the distance between adjacent beads from  $2a$ . The second term is a Lennard-Jones potential that acts between all beads. The strength is given by the parameter  $\tilde{u} = u/(k_B T)$ , which is the dimensionless interaction energy and provides the depth of the bead-bead interaction well. This is normalized by the interaction energy to counteract entropy and collapse a polymer from  $\Theta$ -conditions,  $\tilde{u}_S$ , which defines the collapsing energy  $\Delta\tilde{u} = \tilde{u} - \tilde{u}_S$ . The collapsing behavior of this parameter has been well studied previously,<sup>12,13,16</sup> and we consider only values of  $\tilde{u}$  that are collapsed beyond the  $\Theta$ -condition of the polymer coil. The dynamics of the chain is governed by the Langevin equation

$$\frac{\partial}{\partial t} \mathbf{r}_i = \mathbf{v}_\infty(\mathbf{r}_i) - \sum_j \mu_{ij} \cdot \nabla_{\mathbf{r}_j} U(t) + \xi_i(t), \quad (2)$$

where  $\mathbf{r}_i$  represents the position of bead  $i$ . The mobility matrix  $\mu_{ij}$  accounts for hydrodynamic interactions between particles. We use the well-known Rotne-Prager-Yamakawa tensor,<sup>21,22</sup> which accounts for the finite size of the beads

$$\frac{\mu_{ij}}{\mu_0} = \begin{cases} \frac{3a}{4r_{ij}} \left( \left(1 + \frac{2a^2}{3r_{ij}^2}\right) \mathbf{I} + \left(1 - \frac{2a^2}{r_{ij}^2}\right) \frac{\mathbf{r}_{ij}\mathbf{r}_{ij}}{r_{ij}^2} \right) & r_{ij} \geq 2a \\ \left(1 - \frac{9r_{ij}}{32a}\right) \mathbf{I} + \frac{3}{32} \frac{\mathbf{r}_{ij}\mathbf{r}_{ij}}{ar_{ij}} & r_{ij} \leq 2a, \end{cases} \quad (3)$$

here,  $\xi_i$  is a vectorial random velocity that satisfies  $\langle \xi_i(t) \xi_j(t') \rangle = 6k_B T \mu_{ij} \delta(t - t')$ .

The velocity field  $\mathbf{v}_\infty(\mathbf{r})$  is the undisturbed velocity profile, for which we consider a linear combination of shear and elongation in the x-y plane,

$$\mathbf{v}_\infty(\mathbf{r}) = \left( \begin{bmatrix} 0 & \dot{\gamma} & 0 \\ 0 & 0 & 0 \\ 0 & 0 & 0 \end{bmatrix} + \mathbf{R}(\Theta_0) \begin{bmatrix} \dot{\epsilon} & 0 & 0 \\ 0 & -\dot{\epsilon} & 0 \\ 0 & 0 & 0 \end{bmatrix} \mathbf{R}^{-1}(\Theta_0) \right) \mathbf{r}, \quad (4)$$

where  $\dot{\gamma}$  is the magnitude of the shear flow,  $\dot{\epsilon}$  is the magnitude of the elongational flow, and  $\Theta_0$  is the angle of rotation of the elongational flow profile in the x-y plane with respect to the flow direction of the shear profile (see Fig. 1 for a schematic),

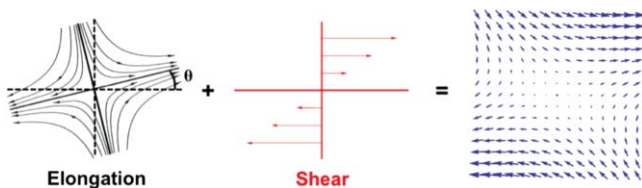


FIG. 1. Schematic demonstrating the relative orientation of the flow profiles. Both an elongational flow field (black streamlines) and a shear flow (red streamlines) can be superimposed. We characterize the relative orientation of the two by rotating the elongational flow field by an angle  $\Theta_0$ .

$\mathbf{R}(\Theta)$  is a rotation matrix given by

$$\begin{bmatrix} \cos(\Theta_0) & -\sin(\Theta_0) & 0 \\ \sin(\Theta_0) & \cos(\Theta_0) & 0 \\ 0 & 0 & 1 \end{bmatrix}. \quad (5)$$

In reality, we have over-parameterized this system; traditionally, it is known that any local two-dimensional flow can be completely described using only a combination of a rotational flow  $\dot{\omega}$  and an elongational flow  $\dot{\epsilon}$ . This is the convention used by the landmark De Gennes paper, and similarly by a number of other authors.<sup>1,23-25</sup> We adopt our equivalent approach, however, to retain a clear connection to the previous work in this area at the limits of no mixing (pure elongation or simple shear). This also allows us to focus on the half of rotation-elongation space where the magnitude of elongation is always larger than the magnitude of the rotation, since if the inverse is true it is well known that stretch transitions cannot occur. This will allow us to examine more clearly the nature of these transitions, since in rotation-elongation space high-shear conditions may lay indistinguishably close to the  $\dot{\epsilon} = \dot{\omega}$  line. Ultimately, we develop this theory such that it is independent of the underlying fluid flow and show that it is applicable regardless of the choice of basis (e.g., for any value of  $\Theta_0$ ). Derivation of the resulting behaviors in the traditional rotation-elongation plane can be trivially accomplished by the replacement  $\dot{\gamma} \rightarrow (1/2)\dot{\omega} + (1/2)\dot{\epsilon}$  for the  $\Theta_0 = \pi/4$  case.

The simulations are performed by integrating a discretized version of Eq. (2) using a time step  $\Delta t = 10^{-4}\tau$ , where  $\tau$  is the characteristic monomer diffusion time  $\tau = a^2/\mu_0 k_B T$ , and  $\mu_0$  is the Stokes mobility of a sphere of radius  $a$ ,  $\mu_0 = 1/(6\pi\eta a)$ , where  $\eta$  denotes the viscosity of the fluid. The total number of Langevin steps simulated at each particular condition is  $3 \times 10^7$ . The starting conformation of the globule is taken from the coordinates of a chain that has been collapsed. The rearrangement time of these globules is typically  $< 10^6$  simulation steps, so we consider the properties of the globule in each simulation to be independent of the initial conformation.

## II. THEORY OF GLOBULE-STRETCH TRANSITIONS

Previous work has elucidated the response of a collapsed polymer coil to the presence of a simple shear and elongational flow.<sup>12-16</sup> Here, we intend to express this theory in a more general sense which presents the essential features of this transition independently from the character of the applied flow field. The critical conceptual picture concerns the transitions between two distinct conformational states: the collapsed state and the stretched state. We draw the analogy to a reversible chemical reaction between two states and define a transition probability for the forward (globule-stretch)  $P_{g-s}$  and backward (tumbling-relaxation)  $P_{s-g}$  reaction. By understanding the relative magnitude of these transition probabilities, the conformational behavior of a globule in an arbitrary fluid flow can be fully described. In the following theory, we separately address both the globule-stretch and tumbling-relaxation transitions.

### A. Globule stretch transition: Nucleation-protrusion mechanism

Previous investigation by Alexander-Katz and Netz has proposed the presence of a nucleation-driven globule unraveling process that drives globule-stretch transitions in fluid flows.<sup>12,13</sup> This theory is based on the notion that the influence of a flow on the geometry of a spherical globule is largely suppressed by the presence of hydrodynamic screening effects. This effect is observed in simulations where hydrodynamic interactions (HI) can be turned off, and the absence of these interactions results in the induction of globule-stretch transitions at significantly lower flow rates.<sup>13,16</sup> For simulations with HI, these transitions occur only through a strictly defined conformational trajectory characterized by the presence of a protruding chain end or loop. This protrusion extends away from the region of hydrodynamic stagnation, and if it is sufficiently long it can be pulled from the globule surface to stretch the polymer. Consequently, if one considers the relevant trajectory through conformational space to be defined by the protrusion contour length, a straightforward nucleation-growth picture emerges upon considering the potentials due to cohesive forces and flow forces (see Fig. 2 for a schematic).

In developing this theory, we will make the assumption that the protruding chain segments from the globule surface are completely thermal and independent of the fluid flow. While this is an approximation, comparison of our numerical results to the resulting analytical predictions demonstrates no considerable difference, which implies that the flow does not have a major role in the protrusion distribution. We also hypothesize a form for the energy of such a potential  $\tilde{U}_{\text{coh}}$ , represented in dimensionless form

$$\tilde{U}_{\text{coh}} \sim \Delta\tilde{u}\tilde{l}^2, \quad (6)$$

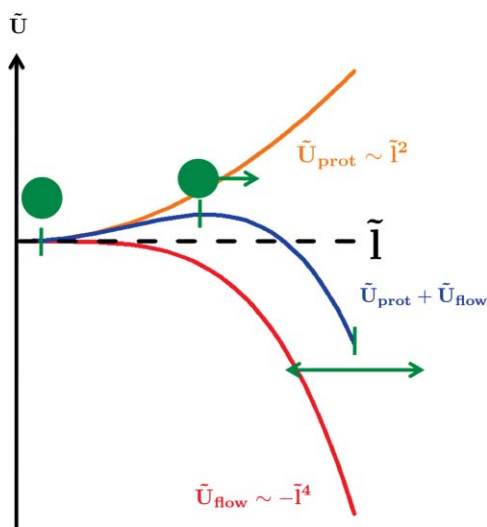


FIG. 2. Schematic demonstrating the nucleation-protrusion stretching mechanism. There is a harmonic increase in energy upon stretching a protrusion of length  $\tilde{l}$  from the surface of a globule. There is increasing drag force on a protrusion as the  $\tilde{l}$  increases due to the increase in fluid flow away from the globule. Once the protrusion is above a critical length, this drag force overcomes the cohesive force and stretching occurs. The green diagrams demonstrate the polymer conformation at that given point along  $\tilde{l}$ .

where  $\Delta\tilde{u}$  is the reduced Lennard-Jones interaction parameter and  $\tilde{l}$  is the length of a thermal protrusion measured from the globule surface. Dimensionless variables are designated with a tilde, and lengths are normalized by a single bead radius  $a$ , energies by the thermal energy  $k_B T$ , and time by the monomer diffusion time  $\tau$ . The form of the potential in Eq. (6) relates to the harmonic approximation that has previously shown to be accurate within the regimes of  $\tilde{u}$  of interest for small values of  $\tilde{l}$ . This protrusion energy allows a simple representation of the protrusion length distribution function  $P(\tilde{l})$ ,

$$P(\tilde{l}) \sim e^{-\Delta\tilde{u}\tilde{l}^2}. \quad (7)$$

This probability distribution function of the protrusion length is useful in characterizing the likelihood of surpassing the critical protrusion length  $\tilde{l}^*$  above which the flow field is strong enough to overcome the globule cohesion. This criterion for  $\tilde{l}^*$  is mathematically represented as

$$f_{\text{coh}}(\Delta\tilde{u}, \tilde{l}^*) \sim f_{\text{flow}}(\dot{m}\tau, N, \tilde{l}^*), \quad (8)$$

where  $f_{\text{coh}} = -\nabla_{\tilde{l}}\tilde{U}_{\text{coh}}$  is the cohesive force that acts to decrease the length of the protrusion  $\tilde{l}$ ,  $f_{\text{flow}}$  is the friction force along the contour of the protrusion that drives it towards the stretched state, and is a function of the flow field (here represented generally by  $(\dot{m}\tau)$ , where  $\dot{m}$  represents an arbitrary fluid flow profile), and chain length  $N$ . The probability of having a protrusion that is longer than  $\tilde{l}^*$  and consequently will undergo a globule-stretch transition is given by

$$P(\tilde{l} > \tilde{l}^*) = \frac{\int_{\tilde{l}^*}^{\infty} e^{-\Delta\tilde{u}\tilde{l}^2} d\tilde{l}}{\int_0^{\infty} e^{-\Delta\tilde{u}\tilde{l}^2} d\tilde{l}} = \text{Erfc}(\sqrt{\Delta\tilde{u}\tilde{l}^*}), \quad (9)$$

where  $\text{Erfc}$  is the complementary error function. Likewise, the average protrusion  $\langle\tilde{l}\rangle$  is given by

$$\langle\tilde{l}\rangle = \frac{\int_0^{\infty} \tilde{l} e^{-\Delta\tilde{u}\tilde{l}^2} d\tilde{l}}{\int_0^{\infty} e^{-\Delta\tilde{u}\tilde{l}^2} d\tilde{l}} = \frac{1}{\sqrt{\pi\Delta\tilde{u}}}. \quad (10)$$

We point out that the limits of integration for both Eqs. (9) and (10) go to infinity, which is clearly unphysical for a polymer of finite length and also does not satisfy the small- $\tilde{l}$  assumption of Eq. (6). The deviations that arise from such an approximation, however, are not significant so long as  $\tilde{u}$  is large enough that  $P(\tilde{l})$  decays rapidly to zero with increasing  $\tilde{l}$ . We consider this condition to be met in a collapsed polymer, but this explains why this theory would no longer be applicable in the case of a  $\Theta$ -polymer.

Up to this point, there has been no specification of the geometry of this protrusion, except that it is a chain end that proceeds from the surface. We continue this derivation, but now with specific reference to the geometry of the protrusion. First, we consider the relevant protrusions to extend radially from the surface of the globule, since these will feel the maximal amount of drag forces due to the fluid flow. The only remaining parameter to define this geometry is to specify the spatial direction of the protrusion. In the absence of flow, such specification is arbitrary, however in the presence of a flow field the overall transition probability of the globule-stretch transition  $P_{g-s}$  must consider contributions from the entire ensemble of paths through conformational space in a non-trivial fashion. We defined each path by its orientation

$\theta$  (measured from the shear flow direction axis,  $x$ ), and write  $P_{g-s}$  as a summation of the transition probabilities  $P_{g-s,\theta}$  over all directions  $\theta$ . Any number of radial paths defined by their angle  $\theta$  can be taken by the protrusion, which means that the overall probability of a globule-stretch transition is written as

$$P_{g-s} = \sum_{\text{paths } \theta} P_{\theta} P_{g-s,\theta}, \quad (11)$$

where we introduce the probability that the protrusion lies along a given path  $\theta$ ,  $P_{\theta}$ . Thus, the results of a globule-stretch transition is a weighted summation of all possible protrusion paths, with  $\sum_{\text{paths } \theta} P_{\theta} = 1$ .

Since the probability of undergoing a globule-stretch transition  $P_{g-s,\theta}$  is proportional to the prevalence of states above the critical protrusion length, Eqs. (9) and (10) combine to yield the probability that a polymer globule can undergo a globule-stretch transition

$$P_{g-s,\theta} \sim P(\tilde{l} > \tilde{l}^*) \sim \text{Erfc} \left( \frac{\tilde{l}^*}{\sqrt{\pi} \langle \tilde{l} \rangle} \right). \quad (12)$$

We invoke the earlier assumption that the value for  $\langle \tilde{l} \rangle$  is entirely thermal and consequently independent of the fluid flow and define the globule-stretch transition as occurring under critical flow conditions  $\dot{m}\tau^*$  defined when  $\tilde{l}^* \sim \langle \tilde{l} \rangle$ .

To determine the dependence of  $\tilde{l}^*$  on fluid flow (and consequently on direction  $\theta$ ), we reintroduce Eq. (8),

$$f_{\text{coh}} = f_{\text{flow},\theta}, \quad (13)$$

which is the condition determined by Alexander-Katz *et al.*<sup>13</sup> From Eq. (6) we can write

$$\tilde{f}_{\text{coh}} \sim \Delta \tilde{u} \tilde{l}, \quad (14)$$

which becomes

$$\tilde{f}_{\text{coh}} \sim \sqrt{\Delta \tilde{u}}, \quad (15)$$

using the relationship  $\langle \tilde{l} \rangle \sim 1/\sqrt{\Delta \tilde{u}}$  derived in Eq. (10), which is assumed to be independent of the fluid flow. Here,  $f_{\text{flow},\theta}$  is the force on the protrusion due to the drag induced by the fluid flow along the direction  $\theta$ . This is given generally in both Refs. 13 and 16 as proportional to the difference between the fluid velocity  $\vec{v}$  at a given position along the chain contour  $\tilde{l}'$  and the fluid velocity at the surface of the globule  $\vec{v}_{\tilde{R}}$  at position  $\tilde{l}' = 0$ ,

$$f_{\text{flow},\theta} = \frac{1}{\mu_0 a} \int_{\tilde{R}}^{\tilde{R}+\tilde{l}} (\vec{v} - \vec{v}_{\tilde{R}}) \cdot d\tilde{l}', \quad (16)$$

where  $\mu_0$  is the hydrodynamic Stokes mobility and  $a$  is a monomer radius. This is therefore the drag force integrated on a path from the surface of the globule  $\tilde{R}$  to the end of the protrusion  $\tilde{R} + \tilde{l}$ , assuming an external velocity field given by  $\vec{v}$  that is taken with reference to the globule surface velocity  $\vec{v}_{\tilde{R}}$ . Along a given path  $\theta$ , we perform an integration through the flow field immediately surrounding a solid sphere. These yield results that follow the form

$$f_{\text{prot}} \sim \alpha(\dot{m}, \theta) l^3 / (a \mu_0 R), \quad (17)$$

where  $\alpha(\dot{m})$  is a function that depends on the flow field  $\dot{m}$  and the path  $\theta$ . For example,  $\alpha = \dot{\gamma}\tau$  along the path  $\theta = \pi/4$  for

simple shear and  $\alpha = \dot{\epsilon}\tau$  along the path  $\theta = 0$  for pure elongation. Since the protrusion force at transition is equivalent to  $f_{\text{coh}}$  which is independent of flow, we can rewrite Eq. (12) as

$$P_{g-s,\theta} \sim \text{Erfc} \left( \left( \frac{\alpha^*}{\alpha} \right)^{1/3} \right), \quad (18)$$

where  $\alpha^*$  is the transition flow rate that is determined upon solving Eq. (8),

$$\dot{m}\tau^* \sim \Delta \tilde{u}^2 R/a. \quad (19)$$

While in principle there are a large number of possible paths  $\theta$ , there are typically two terms that dominate the summation in Eq. (11); the term that corresponds to the maximum  $P_{g-s,\theta}$  and the one that corresponds to the maximum  $P_{\theta}$ . The former is the dominant mechanism in shear globule-stretch transitions, since the rotational flow drives the globule protrusion to sample all values of  $\theta$  equally. We dub this ‘‘transient’’ direction, since a protrusion along this direction is unstable to the rotational component of the fluid flow. The latter is the dominant mechanism in elongational globule-stretch transitions, since the elongational flow profile creates a deep energy well in which the protrusion resides. Thus, regardless of the direction of maximal flow, the protrusion will always follow this path. We dub this ‘‘quasi-static’’ direction, since the protrusion can only leave this well through thermal fluctuations. We consider a two-state model where the globule is in either the quasi-static or transient states, and rewrite Eq. (11) as

$$P_{g-s} = P_0(P_{qs}P_{g-s,qs} + P_{tr}P_{g-s,tr}), \quad (20)$$

where  $P_{qs} + P_{tr} = 1$  and are the relative probabilities of being in either the quasi-static or transient states, respectively. Here,  $P_0$  is a term which indicates the probability that there is an existing protrusion, and that it is along either the quasi-static or the transient directions. In the analytical results presented in this paper, these paths are approximated using the unperturbed flow field (one that does not account for the presence of the globule), where the maximum velocity in the radial direction gives the path to calculate  $P_{tr}$  and the zero velocity in the angular direction gives the path to calculate  $P_{qs}$ .<sup>13,16</sup> A full calculation of the transition pathways would consider the hydrodynamic flow around the polymer globule rather than the unperturbed flow field, however, this is analytically tedious (albeit entirely possible to calculate numerically). Despite the use of this approximation, the analytical results presented later in this paper demonstrate good agreement with simulation results.

## B. Tumbling to non-tumbling transition

Once a polymer globule is stretched, the stability of its extended state is a strong function of the external fluid flow field. In the case of simple shear and elongation, it is well known that the former demonstrates tumbling behavior and the latter remains fully extended. More generally, local flow fields that possess combinations of shear and elongation demonstrate one of these two behaviors based on the characteristics of the flows. We predict that there will be a

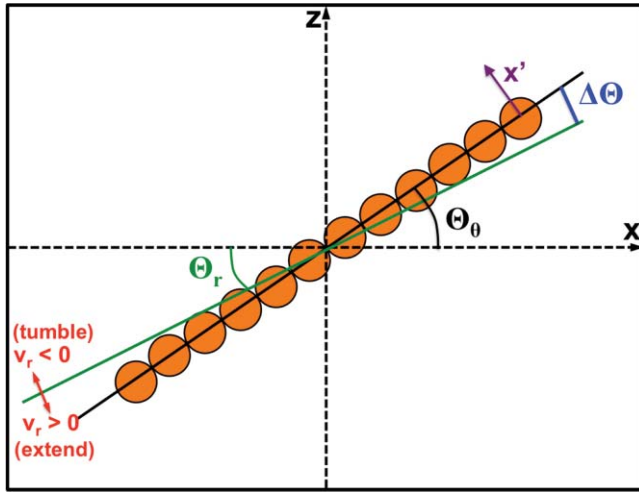


FIG. 3. A schematic of the variables defined in the derivation of the conditions for the tumbling to non-tumbling transition. A chain of  $N$  beads with  $a$  radius that is elongated will equilibrate at an angle  $\Theta_\theta$  that is defined as the angle where the angular component of the velocity field  $v_\theta = 0$ . There is also some angle  $\Theta_r$ , where the radial component of the velocity field  $v_r = 0$ . These are separated by an angle  $\Delta\Theta$ . If  $\Delta\Theta$  is small such that thermal fluctuations can cause the chain to cross into the regime where  $v_r < 0$ , then tumbling behavior will occur.

sharp transition between a tumbling and a non-tumbling state based solely on the flow geometry and a simple statistical mechanical argument. Here, we expand on ideas developed for coils by Woo and Shaqfeh to describe a tumbling-non-tumbling transition in any local fluid flow for both globules and coils.<sup>23</sup>

Both shear and elongational flows can be expressed in terms of polar coordinates, with a separable dependence on the radius  $r$  from a reference point and orientation angle  $\theta$ . In principle, this can be further generalized for three-dimensional flows by including another angle  $\phi$ ; however, we do not consider this here as the conceptual picture remains the same. We can define a coordinate system such as the type shown in Fig. 3, which demonstrates an extended polymer chain in the presence of a mixed fluid flow. We can effectively ignore effects due to hydrodynamic interactions, since the polymer chain is extended. This polymer will be driven to an angle  $\Theta_\theta$  such that it satisfies the following conditions:

$$v_\theta(\Theta_\theta) = 0, \quad (21)$$

$$\left. \frac{\partial v_\theta(\Theta_\theta)}{\partial \theta} \right|_r \leq 0, \quad (22)$$

where  $v_\theta$  is the applied fluid velocity in the  $\theta$  direction. The first condition states that the flow velocity, and consequently the fluid force, in the angular direction has to be zero, otherwise the polymer would be driven to some other angle. The second condition states that if the angular force were represented as a potential  $f_{\text{flow},\theta} = v_\theta/\mu_0 \sim -\partial U_\theta/\partial \theta$ , we are at a local stable extrema ( $\partial^2 U_\theta/\partial \theta^2 > 0$ ). We can also define the critical angle  $\Theta_r$ , where there is a change in the radial velocity is zero,

$$v_r(\Theta_r) = 0, \quad (23)$$

where  $v_r$  is the applied fluid velocity in the radial direction. This condition represents the change from a flow that will extend the polymer ( $v_r > 0$ ) and a flow that will drive a polymer towards collapse ( $v_r < 0$ ). An extended polymer at  $\Theta_\theta$  will thus be in an extended state, unless the chain angle crosses  $\Theta_r$  into a regime where  $v_r < 0$ , which can happen spontaneously due to thermal fluctuations. We can thus characterize the tendency of a polymer in an arbitrary fluid flow by the difference  $\Delta\Theta = \Theta_\theta - \Theta_r$ . There is some critical  $\Delta\Theta^* \sim \delta\theta_P$  where the thermal fluctuations of the polymer  $\delta\theta_P$  are just large enough to allow tumbling to occur. We can create an expansion to second order of the potential that describes the local energy environment around the bead at the end of the elongated chain,

$$U_\theta(\Theta_\theta + \delta\theta_P) = U_\theta(\Theta_\theta) + \left. \frac{\partial U_\theta}{\partial \theta} \right|_{\Theta_\theta} \delta\theta_P + \frac{1}{2} \left. \frac{\partial^2 U_\theta}{\partial \theta^2} \right|_{\Theta_\theta} \delta\theta_P^2, \quad (24)$$

where we consider the contribution to the potential of this bead due to the flow field in the angular ( $U_\theta$ ) direction. This is simplified by considering a redefined  $\Delta U(\delta\theta) = U(\Theta_\theta + \delta\theta) - U_\theta(\Theta_\theta)$ , and realizing based on previous constraints that  $(\partial U_\theta/\partial \theta)|_{\Theta_\theta} = 0$  and  $(\partial^2 U_\theta/\partial \theta^2)|_{\Theta_\theta} = -\partial v_\theta/\mu_0 Na \partial \theta$ . We change to a local cartesian coordinate system through the transformation  $\partial/\partial \theta \sim Na \partial/\partial x'$ ,

$$\Delta U(x') = \frac{1}{2} \left. \frac{\partial^2 U_\theta}{\partial x'^2} \right|_{\Theta_\theta} x'^2 = -\frac{1}{2\mu_0} \left. \frac{\partial v_\theta}{\partial x'} \right|_{\Theta_\theta} x'^2, \quad (25)$$

where  $x'$  is the spatial coordinate in the  $\theta$  direction at  $\Theta_\theta$  (see Fig. 3). We can thus determine the distance of the fluctuation of the chain ends

$$\langle x'^2 \rangle^{1/2} = \left[ \int_{-\infty}^{\infty} x'^2 e^{-\Delta U(x')/kT} dx' \right]^{1/2} \sim \left( \frac{-2kT\mu_0}{(\partial v_\theta/\partial x')|_{\Theta_\theta}} \right)^{1/2}. \quad (26)$$

The condition for tumbling is

$$\langle x'^2 \rangle^{1/2} \geq Na \Delta\Theta^*, \quad (27)$$

so at  $\langle x'^2 \rangle^{1/2} \sim Na \Delta\Theta^*$  there is a tumbling-non-tumbling transition. This is a sharp transition, so it is possible to write

$$P_{s-g} \sim \begin{cases} 0 & \left( \frac{-2kT\mu_0}{(\partial v_\theta/\partial x')|_{\Theta_\theta}} \right)^{1/2} < Na \Delta\Theta^* \\ 1 & \left( \frac{-2kT\mu_0}{(\partial v_\theta/\partial x')|_{\Theta_\theta}} \right)^{1/2} \geq Na \Delta\Theta^*. \end{cases} \quad (28)$$

This general scheme will be considered in the context of two-dimensional flows; however, it is a general set of criteria that would also apply to any three-dimensional flow. One only needs to find the orientation of a fully stretched polymer in spherical coordinates  $\Theta_\theta$  and  $\Phi_\phi$  as a function of the specific flow conditions (which can be described as a linear combination of elongation and shear flows in various directions  $\theta$  and  $\phi$ ) as well as the directions  $\Theta_r$  and  $\Phi_r$ , where there is a change from an outward radial flow to an inward radial flow. Two-dimensional, and likely asymmetric, fluctuations around  $\Theta_\theta$  and  $\Phi_\phi$  would need to be considered in relation to the

distance

$$\Delta(\Theta, \Phi) = \sqrt{(\Theta_\theta - \Theta_r)^2 + (\Phi_\phi - \Phi_r)^2}. \quad (29)$$

While such a calculation would likely be tedious to perform analytically, this type of equation could be performed numerically as part of an overall analysis of a complex flow profile.

### III. RESULTS AND DISCUSSION

In Sec. II, we developed a general theory for the behavior of collapsed polymers in fluid flows that sought to explain the behavior of two types of transitions; globule-shear transitions and tumbling-non-tumbling transitions. This framework can be applied to specific cases of mixed flows to obtain a complete description of a collapsed polymer in that given flow. In order to test these predictions, we will use Brownian dynamics simulations as described in Sec. I. We will use a number of relative orientations  $\Theta_0$  of the elongation and shear components of the mixed flow, as demonstrated in Fig. 1, to show that the theory is robust to changes in the description of the flow field.

To probe the average conformation of a chain under a given set of conditions, we look at a single characteristic parameter: the average tensile force between two adjacent monomers  $\langle F_{i,i+1} \rangle = \langle 2\kappa(r_{i,i+1} - 2a) \rangle = \langle F_T \rangle$ . Previous work has used the chain extension length  $R_{\text{ext}} = \langle R_{x,\text{max}} - R_{x,\text{min}} \rangle$ , which is a direct measure of the chain conformation, but the use of  $\langle F_{i,i+1} \rangle$  allows for completely analogous information with better averaging.<sup>13,16</sup> Furthermore,  $\langle F_{i,i+1} \rangle$  is a useful parameter when considering the biological implications of the globule-flow interactions. In particular, there is a strong evidence that vWF bonds via force-mediated bindings, and so-called “catch bonds” that display enhanced binding upon large forces are ubiquitous in nature.<sup>26,27</sup> We note that the key parameter cited in the literature for force-mediated binding (such as that in vWF) is the maximum force along the chain; however, for characterization purposes better averages are obtained with our parameter.<sup>28,29</sup> It has been shown that the force along an extended chain is a predictable function, so we consider these two parameters are intimately linked and equally relevant.<sup>28</sup>

Two sets of simulations were done for each orientation  $\Theta_0$  that correspond to two different initial conditions. The primary results (represented by the contour plots in the upcoming sections) are given with the initial condition that the polymer is a collapsed globule. Different results, however, are obtained if the polymer is already in an extended conformation, and the flow conditions at which the polymer relaxes into a globule state is indicated by a dotted line in the contour plots.

#### A. $\Theta_0 = 0$

We will first consider the case of  $\Theta_0 = 0$ , which is characterized by an elongation direction parallel to the shear flow direction. To describe this type of flow profile,  $\langle F_{i,i+1} \rangle$  is mapped upon adjusting both the magnitude of the elongational flow  $\dot{\epsilon}$  and the shear flow  $\dot{\gamma}$ . This is plotted as a contour

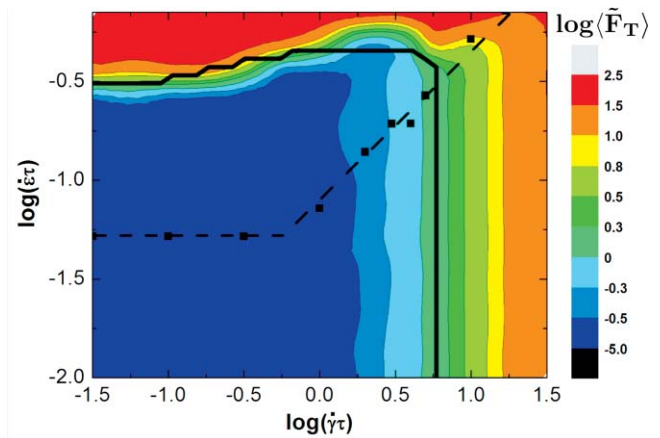


FIG. 4. The tensile-force contour plots within  $\dot{\epsilon}$ - $\dot{\gamma}$  space for  $\Theta_0 = 0$ . The dark line corresponds to Eq. (52). There is good agreement between these values and the apparent globule-stretch transitions. Dotted lines correspond to the relaxation transition, which at high values of  $\dot{\gamma}$  is due to tumbling behavior and at low values of  $\dot{\gamma}$  is due to entropic relaxation. The tumbling behavior follows the scaling derived in Eq. (54), while the black dots represent simulation data. See Fig. 6 for more data on these transitions,  $N = 50$  and  $\Delta\tilde{u} = 1.5$ .

plot in Fig. 4. Also, we indicate the apparent globule-stretch transitions with bold lines. We note that these transitions correspond well to the behavior of  $\langle R_{\text{ext}} \rangle = \langle R_{x,\text{max}} - R_{x,\text{min}} \rangle$ , with states of high tensile forces corresponding directly to states with highly extended conformations. We verify this by plotting data from previous papers of Sing, Alexander-Katz, and Netz that use chain dimensions as the measured parameter along with data for this paper using tensile force data in Fig. 5.<sup>12,13,16</sup>

There is yet another transition that is apparent in the  $\langle F_{i,i+1} \rangle$  contours, which we indicate with a dotted line.

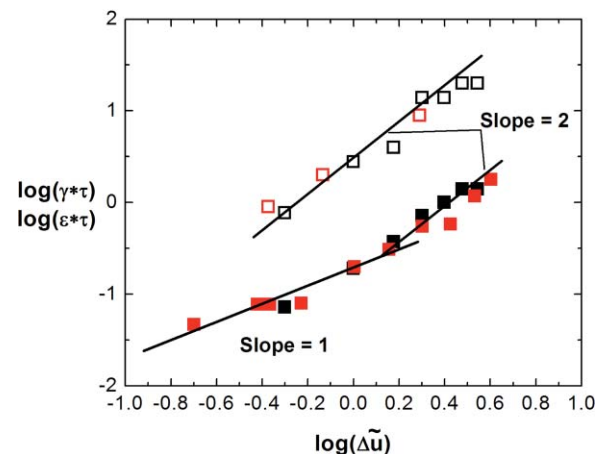


FIG. 5. The critical elongational rate  $\dot{\epsilon}^*\tau$  (solid symbols) and critical shear rate  $\dot{\gamma}^*\tau$  (open symbols) as a function of the interaction energy  $\Delta\tilde{u}$ . We plot the results given in the literature for both  $\dot{\epsilon}^*\tau$  and  $\dot{\gamma}^*\tau$  using the same simulation methods used in this paper (red symbols).<sup>13,16</sup> We include in this plot the critical flow rates for mixed flows in the limit of zero shear flow (solid, black symbols) and zero elongational flow (open, black symbols) determined in the simulations for this paper. As expected, these results correspond directly to the data presented in the existing literature and also follow the scaling behavior derived in each case ( $\Delta\tilde{u} \sim \dot{m}^*\tau$  for both elongation and shear flows in the high- $\Delta\tilde{u}$  regime, and  $\Delta\tilde{u} \sim \dot{\epsilon}^*\tau$  in the low- $\Delta\tilde{u}$  regime).<sup>13,16</sup>

Above the globule-stretch transition, this line corresponds to a tumbling-non-tumbling transition, and below the transition this line indicates the point below which an extended chain can relax back to a globule. Four distinct regions become apparent in this diagram.

At low shear and low elongational flow rates, the average tension force  $\langle F_{i,i+1} \rangle$  is low and represents the region where the polymer chain is in the collapsed globule state regardless of initial condition ( $P_{g-s} \approx 0$  and  $P_{s-g} \approx 1$ ). At regions of higher elongational flow rates, there is a transition to a region where  $\langle F_{i,i+1} \rangle$  is still low if the initial condition of the polymer is a globule, but the polymer cannot relax from an extended conformation ( $P_{g-s} \approx 0$  and  $P_{s-g} \approx 0$ ). Upon increasing the elongation, the globule-stretch transition occurs and there is a region where the polymer is always extended ( $P_{g-s} \approx 1$  and  $P_{s-g} \approx 0$ ). Finally, at low elongation rates and high shear rates the polymer undergoes tumbling behavior ( $P_{g-s} \approx 1$  and  $P_{s-g} \approx 1$ ).

These boundaries are defined by the general theory that was previously developed. For the globule-stretch transitions, we introduce the velocity field surrounding a spherical object. This approach is the same as in previous work; however, here we write these velocity fields in polar coordinates for convenience,<sup>13,16</sup>

$$\tilde{v}_{r,s} = \dot{\gamma} \tau R \tilde{r} \left[ \frac{5 - 7\tilde{r}^2 + 2\tilde{r}^7}{4\tilde{r}^7} \right] \sin(2\theta), \quad (30)$$

$$\tilde{v}_{r,e} = \dot{\epsilon} \tau R \tilde{r} \left[ \frac{(\tilde{r} - 1)^2(3 + 6\tilde{r} + 4\tilde{r}^2 + 2\tilde{r}^3)}{2\tilde{r}^5} \right] \cos(2(\theta - \Theta_0)), \quad (31)$$

$$\tilde{v}_{\theta,s} = -\dot{\gamma} \tau R \frac{\tilde{r}}{2} \left[ 1 - \left( \frac{\tilde{r}^5 - 1}{\tilde{r}^5} \right) \cos(2\theta) \right], \quad (32)$$

$$\tilde{v}_{\theta,e} = -\dot{\epsilon} \tau R \tilde{r} \left[ \frac{4\tilde{r}^7 - 10\tilde{r}^4 + 21\tilde{r}^2 - 15}{4\tilde{r}^7} \right] \sin(2(\theta - \Theta_0)), \quad (33)$$

where  $\tilde{r} = r/R$  and  $v_{i,m}$  the  $i$  component of the velocity vector for the velocity field type  $m$  ( $e$  for elongational and  $s$  for simple shear). The globule-stretch transitions for the simple shear and pure elongation rates must be the limiting case of the other flow component going to zero (at the intercepts of Fig. 4). We show that this is indeed the case in Fig. 5, which graphs both the intercepts of the contour plot and the data from the literature, with both sets of data in agreement.<sup>13,16</sup>

We can use these equations as the inputs for the general theory, but we must choose the correct path along which the protrusion occurs. Naively, this would be the path of maximum drag; however, this needs to be weighted by the probability that the given path would occur as given in Eq. (11). We apply this formalism to this particular case: in the elongation-based globule-stretch transition, there is a large energy well for a protrusion along the path defined by  $\theta = 0$ . This means that a chain end will linger at this position for a while, and occasionally (with a frequency depending on the magnitude of the angular potential) overcome a barrier and circle around the globule. There is thus a decreasing probability of extension at

higher shear rates, since the rotational component of the shear flow allows the protrusion to overcome these barriers. We can develop a two-state model that considers the globule to be in either a quasi-static state that sits in this energy well ( $\theta \sim 0$ ) or a state that is transient ( $\theta \neq 0$ ).

The quasi-static state is characterized by the direction  $\theta = 0$ , and we calculate the total drag force on a protrusion along this direction. Integrating along this path and expanding around  $\tilde{l} \sim 0$ , we obtain the result

$$\tilde{f}_{\text{prot}} = \int_R^{R+\tilde{l}} \left( \tilde{v}_{r,s}(\theta = 0, \tilde{r}) + \tilde{v}_{r,e}(\theta = 0, \tilde{r}) \right) d\tilde{r} \sim \dot{\epsilon} \tau \tilde{l}^3 / \tilde{R}, \quad (34)$$

which is simply the result given in Eq. (17). It thus follows that, for this path

$$P_{g-s,qs} = \text{Erfc} \left( \frac{(\dot{\epsilon} \tau^*)^{1/3}}{(\dot{\epsilon} \tau)^{1/3}} \right), \quad (35)$$

where  $\dot{\epsilon} \tau^* \sim \Delta \tilde{u}^2 R/a$ .

For the transient state, where the protrusion is along  $\theta \neq 0$ , we calculate the total drag force along the protrusion in the direction of maximum drag. We integrate along the path of  $\theta = \pi/4$  to obtain

$$\tilde{f}_{\text{prot}} = \int_R^{R+\tilde{l}} \left( \tilde{v}_{r,s}(\theta = \pi/4, \tilde{r}) + \tilde{v}_{r,e}(\theta = \pi/4, \tilde{r}) \right) d\tilde{r} \sim \dot{\gamma} \tau \tilde{l}^3 / \tilde{R}, \quad (36)$$

which again is the result given in Eq. (17) and is the result for a simple shear flow. It follows:

$$P_{g-s,tr} = \text{Erfc} \left( \frac{(\dot{\gamma} \tau^*)^{1/3}}{(\dot{\gamma} \tau)^{1/3}} \right), \quad (37)$$

where  $\dot{\gamma} \tau^* \sim \Delta \tilde{u}^2 R/a$ .

The amount of time that is spent in the quasi-static versus the transient state can be roughly described using a simple statistical mechanical model. We consider that the probability of finding the protrusion in the quasi-static state is a function of the potential barrier to leave this state and enter the transient state. As an approximation, we consider the barrier to go from the state at  $\Theta_\theta$  to  $\Theta_r$  as defined by the infinite fluid fields

$$\tilde{v}_{r,s} = \frac{\dot{\gamma} \tau \tilde{R} \tilde{r}}{2} \sin(2\theta), \quad (38)$$

$$\tilde{v}_{\theta,s} = -\frac{\dot{\gamma} \tau \tilde{R} \tilde{r}}{2} [1 - \cos(2\theta)], \quad (39)$$

$$\tilde{v}_{r,e} = \dot{\epsilon} \tau \tilde{R} \tilde{r} \cos(2(\theta - \Theta_0)), \quad (40)$$

$$\tilde{v}_{\theta,e} = -\dot{\epsilon} \tau \tilde{R} \tilde{r} \sin(2(\theta - \Theta_0)). \quad (41)$$

These fluid flows can be used to define potential along the  $\theta$  direction by performing an integration in the angular direction

$$\tilde{U}_\theta = -\tilde{\mu}^{-1} \int_{\theta_0}^{\theta} (\tilde{v}_{\theta',s} + \tilde{v}_{\theta',e}) \tilde{R} d\theta', \quad (42)$$

where we can approximate  $\tilde{\mu}$  by the FD value  $\tilde{\mu} = 1$ . The picture is thus of the protrusion as a “bead” at the surface of the globule sphere that explores the energy landscape created by the application of the fluid forces in the  $\theta$  direction. Performing this integration and disregarding the additive constant, we obtain an equation for this energy landscape

$$\tilde{U}_\theta = \gamma\tau\tilde{R}^2\frac{\tilde{r}}{2}\left[\theta - \frac{1}{2}\sin(2\theta)\right] - \dot{\epsilon}\tau\tilde{R}^2\frac{\tilde{r}}{2}\cos(2\theta). \quad (43)$$

This landscape is almost exclusively tilted such that the protrusion rotates (the term linear in  $\theta$ ) in the negative  $\theta$  direction; however, there is a small region between  $\Theta_\theta$  and  $\Theta_r$ , where there is a local minimum in the landscape associated with the quasi-static state. This represents a barrier to constant globule rotation, and the ability of the protrusion to leave this state by overcoming the energetic barrier determines through which route the globule is most likely to extend. Assuming that  $\tilde{r} \sim 1$  and that  $2\theta$  is small, Eq. (43) can be expanded to be

$$\tilde{U}_\theta \approx \tau\tilde{R}^2\left[\gamma\frac{\theta^3}{3} - \frac{\dot{\epsilon}}{2} + \dot{\epsilon}\theta^2\right]. \quad (44)$$

We are only interested in the change in energy in going from  $\Theta_\theta$  to  $\Theta_r$ , which represents the barrier to leave the quasi-static state and is given by

$$\Delta\tilde{U}_\theta \approx \tau\tilde{R}^2\left[\gamma\frac{\Theta_r^3}{3} + \dot{\epsilon}\Theta_r^2\right] - \tau\tilde{R}^2\left[\gamma\frac{\Theta_\theta^3}{3} + \dot{\epsilon}\Theta_\theta^2\right]. \quad (45)$$

This relationship, as well as the tumbling to non-tumbling transition, is defined by the two angles  $\Theta_\theta$  and  $\Theta_r$ . For determining these angles we again use the velocity fields for the infinite flow fields, since we use the approximation that the polymer in the extended state does not perturb the flow field greatly. We use these flow fields to obtain the critical angles  $\Theta_r$  and  $\Theta_\theta$ . Here,  $\Theta_\theta$  is given by the conditions

$$\begin{aligned} \tilde{v}_\theta(\Theta_\theta) = 0 &= \tilde{v}_{\theta,s} + \tilde{v}_{\theta,e} \\ &= -\dot{\epsilon}\tau R\tilde{r}\sin(2\Theta_\theta) - \frac{\gamma\tau R\tilde{r}}{2}[1 - \cos(2\Theta_\theta)], \end{aligned} \quad (46)$$

$$\frac{\partial\tilde{v}_\theta(\Theta_\theta)}{\partial\theta}\Big|_r = -[2\dot{\epsilon}\cos(2\Theta_\theta) + \gamma\sin(2\Theta_\theta)] < 0. \quad (47)$$

For this geometry, we obtain the result  $\Theta_\theta = 0$ . Here,  $\Theta_r$  is given by the condition

$$\begin{aligned} \tilde{v}_r(\Theta_r) = 0 &= \tilde{v}_{r,s} + \tilde{v}_{r,e} \\ &= \frac{\gamma\tau R\tilde{r}}{2}\sin(2\Theta_r) + \dot{\epsilon}\tau R\tilde{r}\cos(2\Theta_r), \end{aligned} \quad (48)$$

which yields the result

$$\tan(2\Theta_r) = -\frac{2\dot{\epsilon}}{\gamma} \approx 2\Theta_r, \quad (49)$$

where the last relationship is true if  $\gamma \gg \dot{\epsilon}$ . Finally, we get

$$\Delta\Theta = \frac{\dot{\epsilon}}{\gamma}. \quad (50)$$

This is an elegantly simple result, which reinforces the physical picture presented in this paper. At large values of  $\dot{\epsilon}$ , there is a large angular difference  $\Delta\Theta$  between the angle along which the chain is extended and the angle at which the chain will start to tumble. The chance of tumbling is thus very small, and a growing protrusion will almost exclusively reside along the quasi-static angle. As the shear (rotational) character of the flow is increased with increasing  $\dot{\gamma}$ , these angles converge so that  $\Delta\Theta$  becomes negligible with respect to chain end fluctuations. Tumbling can then occur, and a growing protrusion will be continually driven in the negative  $\theta$  direction.

This result enables us to fully develop a model for protrusion in the geometry  $\Theta_0 = 0$ , where we break the globule into two states. The quasi-static state is in a low-energy well and is characterized by elongation-induced globule-stretch transitions. The transient state is a higher energy state above the quasi-static state by  $\Delta\tilde{U}_\theta(\Delta\Theta)$  and is characterized by shear-induced globule-stretch transitions. We can combine Eqs. (45) and (49) to obtain

$$\Delta\tilde{U}_\theta \approx \frac{\tilde{R}^2\dot{\epsilon}^3\tau}{6\gamma^2}. \quad (51)$$

This yields the intuitive result that, as the magnitude of the shear flow tends towards zero, the energy well grows infinitely deep. When the shear flow magnitude tends towards infinity, the energy well becomes negligible. We can thus write out the overall probability of a globule-stretch transition based on Eq. (20),

$$\begin{aligned} P_{g-s} &= P_0(P_{qs}P_{g-s,qs} + P_{tr}P_{g-s,tr}) \\ &= P_0\left[\frac{1}{1 + Ce^{-\Delta\tilde{U}(\Delta\Theta)}}\right]Erfc\left(\frac{(\dot{\epsilon}\tau^*)^{1/3}}{(\dot{\epsilon}\tau)^{1/3}}\right) \\ &\quad + P_0\left[\frac{Ce^{-\Delta\tilde{U}(\Delta\Theta)}}{1 + Ce^{-\Delta\tilde{U}(\Delta\Theta)}}\right]Erfc\left(\frac{(\dot{\gamma}\tau^*)^{1/3}}{(\dot{\gamma}\tau)^{1/3}}\right), \end{aligned} \quad (52)$$

where we introduce a coefficient  $C$  that relates the angular “thickness” of the quasi-static state to the transient state, which is on the order of unity. For all graphs in this paper, we use the value  $C = 5$ . The simulation data describe only the normalized value  $P_{g-s,\Delta t}$ , which additionally considers the finite time scale over which the polymer is observed  $\Delta t$ . This takes into account the observation that the polymer will be more likely to unfold if observed in the same state for longer. If the normalization factor  $P_0$  is chosen to be a constant that also accounts for this finite time scale, the transition probability  $P_{g-s}$  can be arbitrarily chosen to be some small but finite probability, such that there is some iso-probability line that describes the behavior of the globule-stretch transition. Sure enough, this equation yields a form for the overall shape of the lines in Fig. 4 (in this figure we choose  $P_{g-s} = 0.1$  to be the transition point). It becomes apparent that this theory captures the essential physics needed to describe this transition.

The behavior of an extended chain upon undergoing a globule-stretch transition is governed by a tumbling-non-tumbling transition, which is characterized by the magnitude

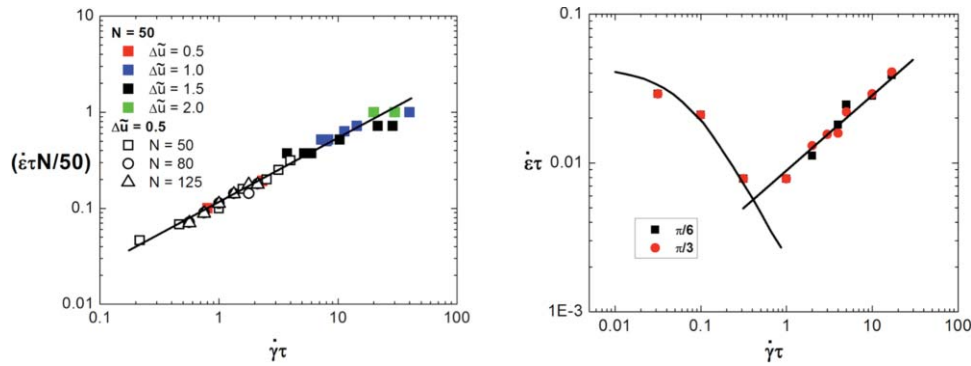


FIG. 6. (a) The tumbling-extension transition as a function of the ( $N = 50$ )-normalized elongation rate  $\dot{\epsilon}\tau N/50$  versus the shear rate  $\dot{\gamma}$  for  $\Theta_0 = 0$ . The fit line represents the predicted scaling of  $\dot{\gamma}^* \sim \dot{\epsilon}^{3/2}$  from Eq. (54), and the simulation data closely follow this trend regardless of the interaction energy  $\Delta\tilde{u}$ . The normalization of  $N/50$  is also predicted by Eq. (54). Solid symbols denote values that are above  $\dot{\gamma}^*$  and  $\dot{\epsilon}^*$  and represent a reversible transition. The open symbols denote values that are below  $\dot{\gamma}^*$  and  $\dot{\epsilon}^*$ . (b) The relaxation transition for  $\Theta_0 = \pi/6$  and  $\pi/3$  mapped on a  $\dot{\epsilon}$ - $\dot{\gamma}$  plot for  $N = 50$ . The relaxation at low values of  $\dot{\gamma}$  are governed by the entropic relaxation time,  $\dot{\epsilon}_r\tau \sim 0.045$ , which is governed by Eq. (83). At high values of  $\dot{\gamma}$ , the relaxation is governed by the tumbling-extension transition. The fit line for this section represents the scaling predicted by Eq. (A14) which is  $\dot{\gamma}^* \sim \dot{\epsilon}^{*2}$ .

of chain-end fluctuations as given by Eq. (26),

$$\langle \tilde{x}^2 \rangle^{1/2} = \left( \frac{-2}{(\partial \tilde{v}_\theta / \partial \tilde{x}')|_{\Theta_\theta}} \right)^{1/2} = \left( \frac{-2N}{(\partial \tilde{v}_\theta / \partial \theta)|_{\Theta_\theta}} \right)^{1/2}. \quad (53)$$

The condition for the tumbling-non-tumbling transition given in Eq. (27) yields the result

$$\dot{\gamma}^* \sim N \dot{\epsilon}^{*3/2} \tau^{1/2}. \quad (54)$$

This scaling is represented in Fig. 4 by the dotted dark line in the large- $\dot{\gamma}$  regime. This line extends below the globule-

stretch transitions, and in this regime represents the line of stability of a previously extended chain. We verify that this scaling holds true for many different values of chain length  $N$  and self-interaction parameters  $\Delta\tilde{u}$ , which is shown in Fig. 6(a). The collapse of all of these different conditions onto the same curve of slope  $2/3$  (predicted above) demonstrates the validity of this theory. This line transitions to having no  $\dot{\gamma}$  dependence at the value of  $\dot{\epsilon}$  that is approximately the inverse relaxation time of a theta polymer, which we dub  $\dot{\epsilon}_r$ . This point represents the extent of the hysteresis for globule-stretch transitions, which is shown in Fig. 6 for a polymer under pure

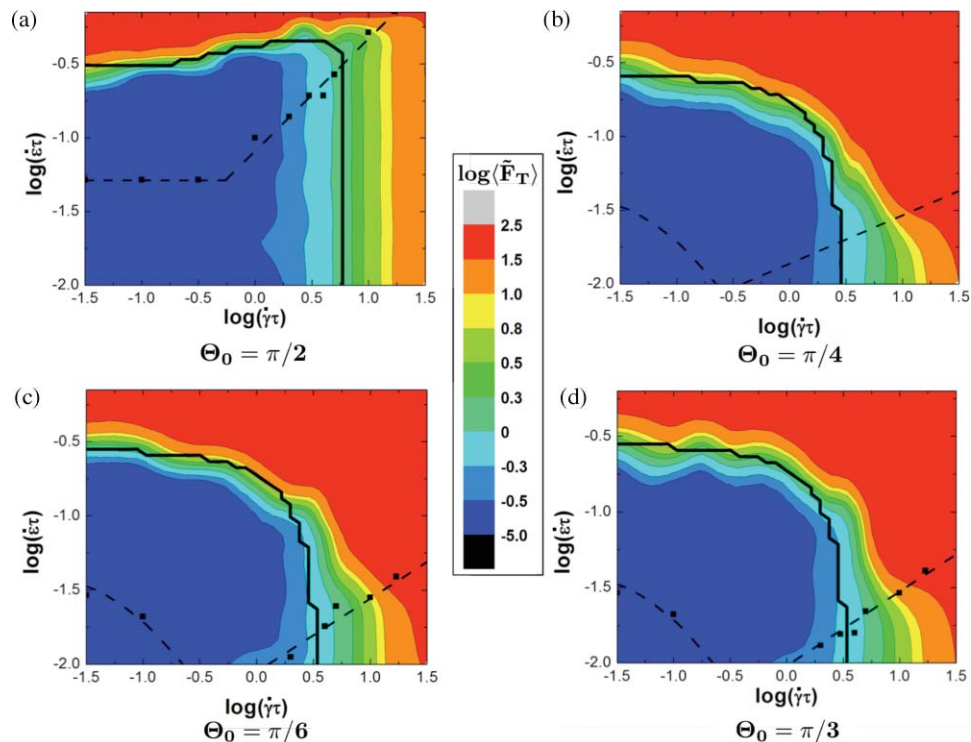


FIG. 7. The tensile-force contour plots within  $\dot{\epsilon}$ - $\dot{\gamma}$  space for  $\Theta_0 = \pi/2$  (a),  $\pi/4$  (b),  $\pi/6$  (c), and  $\pi/3$  (d). Dark lines correspond to Eqs. (69), (81) and (A19) for their respective values of  $\Theta_0$ . There is good agreement between these values and the apparent globule-stretch transitions. Dotted lines correspond to the relaxation transitions, which at high values of  $\dot{\gamma}$  are due to tumbling behavior and at low values of  $\dot{\gamma}$  are due to entropic relaxation. The fit lines represent the scaling seen in Eqs. (72), (A5), (A5), and (A14), while the black dots represent simulation data. See Fig. 6 for more data on these transitions. All plots are for  $N = 50$  and  $\Delta\tilde{u} = 1.5$ .

elongational flow. Both collapsed and theta polymers are shown, and it is clear that while the globule-stretch transition does not depend on the polymer relaxation time, the stretch-globule transition occurs when the polymer just begins to relax. At the initial stages of relaxation, the kinetic pathway towards collapse become available due to the ability of the chain to self-interact. The critical transition elongation rate  $\dot{\epsilon}_r$  is ultimately related to the relaxation time of the polymer, which has been widely studied previously, so we will not discuss this topic at length.<sup>1-5</sup>

## B. $\Theta_0 = \pi/2$

We next consider the case of  $\Theta_0 = \pi/2$ , with the elongation direction perpendicular to the shear flow direction. We again consider a map of  $\langle F_{i,i+1} \rangle$  as a function of  $\log(\dot{\epsilon})$  versus  $\log(\dot{\gamma})$ , which is shown in Fig. 7(a). We also show the apparent globule-stretch transitions and tumbling-non-tumbling transitions in the same way as Fig. 4. Upon decomposing the shear flow into rotation and elongation, it is clear that this geometry is essentially the same as the  $\Theta_0 = 0$  case, albeit rotated by an angle of  $\pi/4$ . This is further illustrated by the fact that Figs. 7(a) and 4 are essentially identical. It is not necessary to realize this equivalence or account for the spatial rotation; however, and we can demonstrate that an analogous derivation again yields the correct result.

To determine the preferred paths for the quasi-static and transient states, we again use the infinite-field assumption to determine the angle of the quasi-static energy well (equivalent to  $\Theta_\theta$ ) and the angle of maximum radial velocity  $\Theta_{max}$ . For the former, we write the conditions

$$\tilde{v}_\theta(\Theta_\theta) = 0 = \dot{\epsilon} \tau R \tilde{r} \sin(2\Theta_\theta) - \frac{\dot{\gamma} \tau R \tilde{r}}{2} [1 - \cos(2\Theta_\theta)], \quad (55)$$

$$\left. \frac{\partial \tilde{v}_\theta(\Theta_\theta)}{\partial \theta} \right|_r = 2\dot{\epsilon} \cos(2\Theta_\theta) - \dot{\gamma} \sin(2\Theta_\theta) < 0, \quad (56)$$

This yields the result

$$\Theta_\theta = \arctan \left[ \frac{2\dot{\epsilon}}{\dot{\gamma}} \right]. \quad (57)$$

To find  $\Theta_{max}$ , we use the condition

$$\left. \frac{\partial \tilde{v}_r}{\partial \theta} \right|_{\Theta_{max}} = 0 = \frac{\dot{\gamma}}{2} \cos(2\Theta_{max}) + \dot{\epsilon} \sin(2\Theta_{max}), \quad (58)$$

which yields the result

$$\Theta_{max} = \frac{1}{2} \arctan \left[ -\frac{\dot{\gamma}}{2\dot{\epsilon}} \right]. \quad (59)$$

The quasi-static state is characterized by the direction  $\Theta_\theta$ , and we calculate the total drag force along this path

$$\begin{aligned} \tilde{f}_{\text{prot}} &= \int_1^{1+\tilde{l}} (\tilde{v}_{r,s}(\Theta_\theta, \tilde{r}) + \tilde{v}_{r,e}(\Theta_\theta, \tilde{r})) d\tilde{r} \\ &\sim \dot{\epsilon} \tau \tilde{l}^3 / \tilde{R}, \end{aligned} \quad (60)$$

which is the same result as in Eq. (34). As in the case of  $\Theta_0 = 0$ , it thus follows that

$$P_{g-s,qs} = \text{Erfc} \left( \frac{(\dot{\epsilon} \tau^*)^{1/3}}{(\dot{\epsilon} \tau)^{1/3}} \right), \quad (61)$$

where  $\dot{\epsilon} \tau^* \sim \Delta \tilde{u}^2 R/a$ . The transient case also behaves similarly to the  $\Theta_0 = 0$  case in the limit of  $\dot{\gamma} \gg \dot{\epsilon}$ . The force along this path is

$$\begin{aligned} \tilde{f}_{\text{prot}} &= \int_1^{1+\tilde{l}} (\tilde{v}_{r,s}(\Theta_{max}, \tilde{r}) + \tilde{v}_{r,e}(\Theta_{max}, \tilde{r})) d\tilde{r} \\ &\sim \dot{\gamma} \tau \tilde{l}^3 / \tilde{R}, \end{aligned} \quad (62)$$

which again is the result given in Eq. (17) and is the result for a simple shear flow. It follows:

$$P_{g-s,tr} = \text{Erfc} \left( \frac{(\dot{\gamma} \tau^*)^{1/3}}{(\dot{\gamma} \tau)^{1/3}} \right), \quad (63)$$

where  $\dot{\gamma} \tau^* \sim \Delta \tilde{u}^2 R/a$ . These results are the same as for  $\Theta_0 = 0$ , despite the change in flow representation.

Here,  $\Theta_r$  can also be calculated, using the condition

$$\tilde{v}_r(\Theta_r) = 0 = \frac{\dot{\gamma} \tau R \tilde{r}}{2} \sin(2\Theta_r) - \dot{\epsilon} \tau R \tilde{r} \cos(2\Theta_r). \quad (64)$$

This yields the result

$$\Theta_r = \arctan \left[ \frac{\sqrt{4 + \dot{\gamma}^2 / \dot{\epsilon}^2} - \dot{\gamma} / \dot{\epsilon}}{2} \right] \approx \arctan \left[ \frac{\dot{\epsilon}}{\dot{\gamma}} \right], \quad (65)$$

where the relationship on the far right is in the limit of  $\dot{\gamma} \gg \dot{\epsilon}$ . Finally, also in this limit, we can write the relationship

$$\Delta \Theta = \Theta_\theta - \Theta_r \approx \frac{\dot{\epsilon}}{\dot{\gamma}}, \quad (66)$$

which is yet again a result identical with the case of  $\Theta_0 = 0$ . We also calculate  $\tilde{U}$  in the same fashion as before and obtain

$$\tilde{U} \approx \tau \tilde{R}^2 \left[ \dot{\gamma} \frac{\theta^3}{3} + \frac{\dot{\epsilon}}{2} - \dot{\epsilon} \theta^2 \right]. \quad (67)$$

Taking the difference  $\Delta \tilde{U}_{\pi/2} = \tilde{U}(\Theta_r) - \tilde{U}(\Theta_\theta)$ ,

$$\Delta \tilde{U}_{\pi/2} \approx \frac{2\tilde{R}^2 \dot{\epsilon}^3 \tau}{3\dot{\gamma}^2}. \quad (68)$$

With this we can write out the full equation for the globule-stretch transition for  $\Theta_0 = \pi/2$ ,

$$\begin{aligned} P_{g-s,u} &= P_{qs} P_{g-s,qs} + P_{tr} P_{g-s,tr} \\ &= \left[ \frac{1}{1 + C e^{-\Delta \tilde{U}_{\pi/2}(\Delta \Theta)}} \right] \text{Erfc} \left( \frac{(\dot{\epsilon} \tau^*)^{1/3}}{(\dot{\epsilon} \tau)^{1/3}} \right) \\ &\quad + \left[ \frac{C e^{-\Delta \tilde{U}_{\pi/2}(\Delta \Theta)}}{1 + C e^{-\Delta \tilde{U}_{\pi/2}(\Delta \Theta)}} \right] \text{Erfc} \left( \frac{(\dot{\gamma} \tau^*)^{1/3}}{(\dot{\gamma} \tau)^{1/3}} \right), \end{aligned} \quad (69)$$

which is essentially equivalent to Eq. (52) for  $\Theta_0 = 0$ , in accordance with the similarity between Figs. 7(a) and 4.

Similarly, the tumbling-non-tumbling transition displays essentially the same behavior in both  $\Theta_0 = 0$  and  $\Theta_0 = \pi/2$ .

We again write the magnitude of chain-end fluctuations

$$\langle \tilde{x}^2 \rangle^{1/2} = \left( \frac{-2N}{(\partial \tilde{v}_\theta / \partial \theta)|_{\Theta_\theta}} \right)^{1/2} \quad (70)$$

and substitute in

$$\frac{\partial \tilde{v}_\theta}{\partial \theta} |_{\Theta_\theta} = -\dot{\gamma} \tau N \sin(2\Theta_\theta) + 2\dot{\epsilon} \tau N \cos(2\Theta_\theta) \approx -2N\dot{\epsilon} \tau, \quad (71)$$

which yields the familiar result for the tumbling-non-tumbling transition

$$\dot{\gamma}^* \sim N \dot{\epsilon}^{3/2} \tau^{1/2}. \quad (72)$$

### C. $\Theta_0 = \pi/4$

The case of  $\Theta_0 = 0$  and  $\Theta_0 = \pi/2$  are analogous to each other, with qualitatively similar behavior that is characterized by roughly independent shear and elongation directions. With the case of  $\Theta_0 = \pi/4$ , we expect cooperative behavior due to the elongational direction of the shear flow being in the same direction as the direction of the elongational flows. Simulations using this geometry demonstrate markedly different behavior in a shear-elongation plane, which is plotted in Fig. 7(b) in the same fashion as Figs. 4 and 7(a). We again demonstrate that this behavior is predicted by our theory. The flow field is now described by

$$\tilde{v}_\theta = \dot{\epsilon} \tau N \cos(2\theta) - \frac{\dot{\gamma} \tau N}{2} [1 - \cos(2\theta)], \quad (73)$$

$$\tilde{v}_r = \dot{\epsilon} \tau N \sin(2\theta) + \frac{\dot{\gamma} \tau N}{2} \sin(2\theta). \quad (74)$$

This results in the following characteristics (with the approximation that  $\dot{\gamma} \gg \dot{\epsilon}$  used appropriately in the same fashion as the above results):

$$\Theta_\theta = \frac{1}{2} \arccos \left[ \frac{\dot{\gamma}}{2\dot{\epsilon} + \dot{\gamma}} \right], \quad (75)$$

$$\Theta_r = 0, \quad (76)$$

$$\Theta_{\max} = \pi/4, \quad (77)$$

$$\Delta \tilde{U}_{\pi/4} \approx \frac{2\tau^{1/2} \tilde{R}^2 \dot{\epsilon}^{3/2}}{3\dot{\gamma}}, \quad (78)$$

$$\tilde{f}_{\text{prot},tr} \sim \frac{5}{2} \tau \tilde{R} \tilde{l}^3 \left( \dot{\epsilon} + \frac{7}{6} \dot{\gamma} \right), \quad (79)$$

$$\tilde{f}_{\text{prot},qs} \sim \begin{cases} \frac{5}{2} \tau \tilde{R} \tilde{l}^3 \left[ \dot{\epsilon} + \frac{7}{6} \dot{\gamma} \right] & \dot{\epsilon} > \dot{\gamma} \\ 5\tau \tilde{R} \tilde{l}^3 \left( \frac{\dot{\epsilon}}{\dot{\gamma}} \right)^{1/2} \left[ \dot{\epsilon} + \frac{7}{6} \dot{\gamma} \right] & \dot{\epsilon} < \dot{\gamma} \end{cases}. \quad (80)$$

This can be combined to yield the results

$$\begin{aligned} P_{g-s} &= P_{qs} P_{g-s,qs} + P_{tr} P_{g-s,tr} \\ &= \left[ \frac{1}{1 + C e^{-\Delta \tilde{U}_{\pi/4}(\Delta \Theta)}} \right] \text{Erfc} \left( \frac{(\dot{\epsilon} \tau^* + 7\dot{\gamma} \tau/6)^{1/3}}{(\dot{\epsilon} \tau + 7\dot{\gamma} \tau/6)^{1/3}} \right) \\ &\quad + \left[ \frac{C e^{-\Delta \tilde{U}_{\pi/4}(\Delta \Theta)}}{1 + C e^{-\Delta \tilde{U}_{\pi/4}(\Delta \Theta)}} \right] \text{Erfc} \left( \frac{(\dot{\epsilon} \tau + 7\dot{\gamma} \tau^*/6)^{1/3}}{(\dot{\epsilon} \tau + 7\dot{\gamma} \tau/6)^{1/3}} \right) \end{aligned} \quad (81)$$

and

$$\dot{\gamma}^* \sim N^4 \dot{\epsilon}^{*3} \tau^2, \quad (82)$$

where the first result simplifies to the equation for pure elongation or shear when a negligible amount of the other component is involved. These results are plotted on the graph in Fig. 7(b). As mentioned previously, it is straightforward to translate these results to describe behaviors in a rotation-elongation plane through the substitution of  $\dot{\gamma} \rightarrow (1/2)\dot{\omega} + (1/2)\dot{\epsilon}$ .

This same process can be used to determine the results for increasingly complex flows, such as the case of  $\Theta_0 = \pi/3$  and  $\pi/6$ , the results of which are included in the Appendix. These results are plotted in Figs. 7(c) and 7(d). The similarity between these two curves again highlights their equivalence upon decomposition to rotational and elongational components in the same fashion as  $\Theta_0 = 0$  and  $\Theta_0 = \pi/2$ .

### D. Relaxation transition

We briefly consider the relaxation of a collapsing polymer in a flow field in the absence of tumbling. Figure 8 demonstrates the hysteresis of a globule-stretch transition in the presence of an elongational flow field. In order for the polymer to retain a globule conformation from a fully stretched conformation, it must relax enough such that there is sufficient chain self-interaction to allow the polymer to realize a kinetically viable relaxation pathway. As demonstrated in Fig. 8, this point occurs when the polymer begins to relax due to an entropic restoring force. Since the critical mechanism is due to the competition of entropic forces and the stretching forces of the fluid flow, we expect this transition to be directly correlated to the coil-stretch transition point that has been widely studied. Since this behavior is well understood, we choose not to investigate this behavior and instead

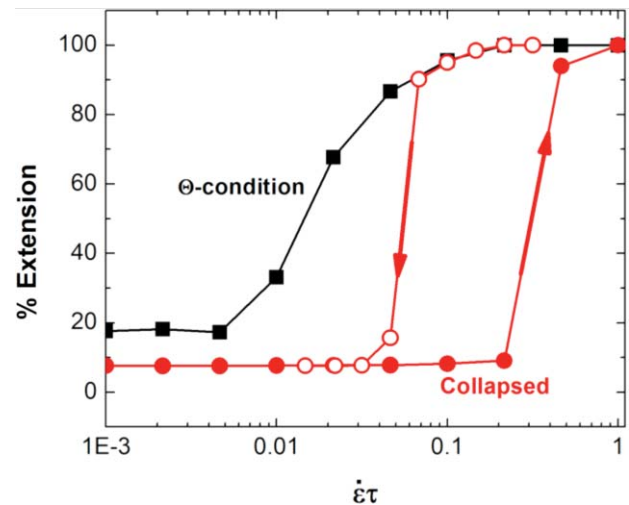


FIG. 8. The hysteresis presents in the stretching and collapsing behavior of a polymer chain with high  $\Delta \tilde{u}$  ( $= 1.5$ ) self-interactions (red). Filled symbols represent increasing  $\dot{\epsilon} \tau$  and open symbols represent decreasing  $\dot{\epsilon} \tau$ . This is compared to the behavior of a chain extending at  $\Theta$ -conditions (black,  $\tilde{u} = 0.41$ ).

simply define a critical elongation rate  $\dot{\epsilon}_r$  that is governed by the characteristic relaxation time of the polymer.

In the case of  $\Theta_0 = 0$  and  $\pi/2$ , this value is independent on the value of the shear rate  $\dot{\gamma}$ . In the cases of  $\pi/4$ ,  $\pi/3$ , and  $\pi/6$ , there is a strong  $\dot{\gamma}$  dependence due to the presence of the elongational component of the shear flows. Using the straightforward relation

$$\dot{\epsilon}_r \sim \frac{\tilde{v}_{r,\Theta_\theta}}{Na}, \quad (83)$$

we can determine the dependence of  $\dot{\epsilon}_r$  on  $\dot{\gamma}$ . These are plotted on Figs. 7(c) and 7(d) at points where it can be seen in the scope of the contour plot. These relations, as well as those for the tumbling-non-tumbling transition, are re-plotted together on Fig. 6(b) to demonstrate the full range of these functions. Clearly, these functions are well described by the theory.

### E. Extension to three dimensions

The flows considered here are two-dimensional since we set the applied flow field in the  $z$  direction to be zero. We expect that the analysis performed here for two-dimensional flows could be applied in exactly the same way to a three-dimensional flow. This type of analysis would be much more computationally taxing, and analytical solutions would be tedious, but not prohibitive. The critical parameters of  $\Theta_\theta$ ,  $\Theta_{\max}$ , and  $\Delta U$  would still govern this behavior; however, they could be at any point along the globule-surface and thus a second angular component would need to be introduced.

### F. Understanding collapsed globules in rheological flows

When the rheological properties of polymers in flow are considered, connections must be made between the microscopic representation of the polymer and the macroscopic properties of the system (most importantly, viscosity). For example, the widely used dumbbell model represents a single polymer chain with a representative “dumbbell,” which consists of two spheres to represent the drag on the polymer due to flow that are connected by a spring that represents relaxation forces (i.e., entropic relaxation and chain connectivity forces at high extensions). The most simple versions of these models are derived from a consideration of the configurational phase space occupied by a polymer and how it will respond to an applied flow field. These models are convenient since they can be analytically incorporated into constitutive equations and applied to real fluid flows.

In this specific case, we provide an example of how a similar connection can be made between the microscopic behaviors described in this paper and the macroscopic rheological properties of a dilute globule solution. We can treat the system, rather than an average over all of phase space, as a linear combination of two discrete states. This is possible since there is a large kinetic barrier that separates two very small areas in phase space—the point that represents the fully—elongated polymer and the area that represents a polymer globule. Dynamically, it is possible to access states in

between these two during transitions; however, we make the assumption that these states are transient and that the overall contribution of these states are negligible. With these considerations, and retaining our assumption of dilute solution, we can simply represent the rheological properties (for example, the polymer contribution to the viscosity  $\eta_P$ ) as a sum of the contributions of stretched polymers ( $\eta_{P,r}$  and collapsed polymers ( $\eta_{P,g}$ ),

$$\eta_P \approx f_r \eta_{P,r} + f_g \eta_{P,g}, \quad (84)$$

where the subscript  $r$  corresponds to the result for a rod polymer and the subscript  $g$  corresponds to the result for a globular polymer. The values  $f_i$  are the fractions of polymers in state  $i$ . The rheological properties of rods and globules are well known, and we will not cover them here.<sup>30</sup> The introduction of our model above is required to find the values of  $f_i$  through the use of the equations

$$f_r(t) = \int_{-\infty}^t [f_g(t') P_{g-s}(\dot{m}(t')) - f_r(t') P_{s-g}(\dot{m}(t'))] dt', \quad (85)$$

$$f_g(t) = \int_{-\infty}^t [-f_g(t') P_{g-s}(\dot{m}(t')) + f_r(t') P_{s-g}(\dot{m}(t'))] dt', \quad (86)$$

where  $P_{g-s}$  and  $P_{s-g}$  represent inputs from the general theory given above, and we reintroduce the general flow function  $\dot{m}$  to represent the local flow conditions.

## IV. CONCLUSION

In conclusion, we have developed a general theory for the behavior of collapsed polymers in mixed elongational and shear flows. This theory is based on the characterization of two “transitions” that can occur between globule and stretched states. In the globule-stretch transition, a thermally activated chain end protruding from the surface must be long enough so that the flow profile around the globule can overcome the cohesive force holding the globule together. Once elongated, the chain can revert to the globule state either through a driven tumbling process or an entropic relaxation process. The criterion for all of these transitions are described in a quantitative fashion and are fit to simulation data for two-dimensional flow fields. Generalizations to three-dimensional flow fields is discussed as is the incorporation of these results into rheological equations for dilute solutions. The existence of large hysteresis effects, especially in the elongation direction, must be taken into account in this case, and such solutions will demonstrate non-trivial memory effects.

The behavior of collapsed homopolymers in flow is becoming increasingly relevant as the importance of globular polymers is being realized; recent work demonstrating the equivalence between homopolymer globules and the quaternary structures of biopolymers, such as vWF has shown both that these types of behaviors can be crucial in biological processes, and furthermore that such physics may be a useful

route to creating switchable polymers that respond to fluid flow stimuli.<sup>13,15</sup>

### APPENDIX: $\Theta_0 = \pi/3, \pi/6$

For the case of  $\Theta_0 = \pi/3$ , we use the same methods used in Secs. III A–III C to obtain

$$\tilde{v}_\theta = -\frac{\dot{\gamma}\tau N}{2} [1 - \cos(2\theta)] + \dot{\epsilon}\tau N \left[ \frac{\sqrt{3}}{2} \cos(2\theta) + \frac{1}{2} \sin(2\theta) \right], \quad (\text{A1})$$

$$\tilde{v}_r = \frac{\dot{\gamma}\tau N}{2} \sin(2\theta) + \dot{\epsilon}\tau N \left[ -\frac{1}{2} \cos(2\theta) + \frac{\sqrt{3}}{2} \sin(2\theta) \right], \quad (\text{A2})$$

$$\Theta_r = \frac{1}{2} \arctan \left[ \frac{\epsilon}{\sqrt{3}\dot{\epsilon} + \dot{\gamma}} \right], \quad (\text{A3})$$

$$\Theta_\theta = \arccos \left[ \left( \frac{2\dot{\gamma}^2 + 4\dot{\epsilon}^2 + 3\sqrt{3}\dot{\epsilon}\dot{\gamma} - \dot{\epsilon}\sqrt{2\sqrt{3}\dot{\epsilon}\dot{\gamma} + 4\dot{\epsilon}^2}}{2\dot{\gamma}^2 + 8\dot{\epsilon}^2 + 4\sqrt{3}\dot{\epsilon}\dot{\gamma}} \right)^{1/2} \right], \quad (\text{A4})$$

$$\Theta_{\max} = \frac{\pi}{2} - \frac{1}{2} \arctan \left[ \frac{\dot{\gamma} + \sqrt{3}\dot{\epsilon}}{\dot{\epsilon}} \right] \dot{\gamma}^* \sim N^2 \dot{\epsilon}^{*2} \tau, \quad (\text{A5})$$

$$\Delta \tilde{U}_{\pi/3} \approx \frac{\tau \tilde{R}^2 \dot{\epsilon}^{3/2}}{\sqrt{2\sqrt{3}} \dot{\gamma}^{1/2}}, \quad (\text{A6})$$

$$\tilde{f}_{\text{prot},qs} \sim \begin{cases} \frac{5}{2} \tau \tilde{R} \tilde{l}^3 \left[ \dot{\epsilon} + \frac{7\sqrt{3}}{12} \dot{\gamma} \right] & \dot{\epsilon} > \dot{\gamma} \\ \frac{5}{2} \tau \tilde{R} \tilde{l}^3 \left[ -\frac{\dot{\epsilon}}{2} + \frac{7\sqrt{2\sqrt{3}}}{3} \dot{\gamma}^{1/2} \dot{\epsilon}^{1/2} \right] & \dot{\epsilon} < \dot{\gamma} \end{cases}, \quad (\text{A7})$$

$$\tilde{f}_{\text{prot},tr} \sim \begin{cases} \frac{5}{2} \tau \tilde{R} \tilde{l}^3 \left[ \dot{\epsilon} + \frac{7\sqrt{3}}{12} \dot{\gamma} \right] & \dot{\epsilon} > \dot{\gamma} \\ \frac{5}{2} \tau \tilde{R} \tilde{l}^3 \left[ \frac{\sqrt{3}}{2} \dot{\epsilon} + \frac{7}{6} \dot{\gamma} \right] & \dot{\epsilon} < \dot{\gamma} \end{cases}. \quad (\text{A8})$$

For the case of  $\Theta_0 = \pi/6$ , we obtain

$$\tilde{v}_\theta = -\frac{\dot{\gamma}\tau N}{2} [1 - \cos(2\theta)] + \dot{\epsilon}\tau N \left[ \frac{1}{2} \cos(2\theta) - \frac{\sqrt{3}}{2} \sin(2\theta) \right], \quad (\text{A9})$$

$$\tilde{v}_r = \frac{\dot{\gamma}\tau N}{2} \sin(2\theta) + \dot{\epsilon}\tau N \left[ \frac{1}{2} \cos(2\theta) + \frac{\sqrt{3}}{2} \sin(2\theta) \right], \quad (\text{A10})$$

$$\Theta_r = \frac{1}{2} \arctan \left[ \frac{-\epsilon}{\sqrt{3}\dot{\epsilon} + \dot{\gamma}} \right], \quad (\text{A11})$$

$$\Theta_\theta = \arccos \left[ \left( \frac{2\dot{\gamma}^2 + 4\dot{\epsilon}^2 + 3\sqrt{3}\dot{\epsilon}\dot{\gamma} + \dot{\epsilon}\sqrt{2\sqrt{3}\dot{\epsilon}\dot{\gamma} + 4\dot{\epsilon}^2}}{2\dot{\gamma}^2 + 8\dot{\epsilon}^2 + 4\sqrt{3}\dot{\epsilon}\dot{\gamma}} \right)^{1/2} \right], \quad (\text{A12})$$

$$\Theta_{\max} = \frac{1}{2} \arctan \left[ \frac{\dot{\gamma} + \sqrt{3}\dot{\epsilon}}{\dot{\epsilon}} \right], \quad (\text{A13})$$

$$\dot{\gamma}^* \sim N^2 \dot{\epsilon}^{*2} \tau, \quad (\text{A14})$$

$$\Delta \tilde{U}_{\pi/6} \approx \frac{\tau \tilde{R}^2 \dot{\epsilon}^{3/2}}{\sqrt{2\sqrt{3}} \dot{\gamma}^{1/2}}, \quad (\text{A15})$$

$$\tilde{f}_{\text{prot},qs} \sim \begin{cases} \frac{5}{2} \tau \tilde{R} \tilde{l}^3 \left[ \dot{\epsilon} + \frac{7\sqrt{3}}{12} \dot{\gamma} \right] & \dot{\epsilon} > \dot{\gamma} \\ \frac{5}{2} \tau \tilde{R} \tilde{l}^3 \left[ \frac{\dot{\epsilon}}{2} + \frac{7\sqrt{2\sqrt{3}}}{6} \dot{\gamma}^{1/2} \dot{\epsilon}^{1/2} \right] & \dot{\epsilon} < \dot{\gamma} \end{cases}, \quad (\text{A16})$$

$$\tilde{f}_{\text{prot},tr} \sim \begin{cases} \frac{5}{2} \tau \tilde{R} \tilde{l}^3 \left[ \dot{\epsilon} + \frac{7\sqrt{3}}{12} \dot{\gamma} \right] & \dot{\epsilon} > \dot{\gamma} \\ \frac{5}{2} \tau \tilde{R} \tilde{l}^3 \left[ \frac{\sqrt{3}}{2} \dot{\epsilon} + \frac{7}{6} \dot{\gamma} \right] & \dot{\epsilon} < \dot{\gamma} \end{cases}. \quad (\text{A17})$$

These again can be considered with the general format

$$P_{g-s} = P_{qs} P_{g-s,qs} + P_{tr} P_{g-s,tr}, \quad (\text{A18})$$

which can be approximated as

$$P_{g-s} = P_{qs} P_{g-s,qs} + P_{tr} P_{g-s,tr} = \left[ \frac{1}{1 + C e^{-\Delta \tilde{U}_{\pi/6}(\Delta \Theta)}} \right] \text{Erfc} \left( \frac{(\dot{\epsilon}\tau^* + 7\sqrt{3}\dot{\gamma}\tau/12)^{1/3}}{(\dot{\epsilon}\tau + 7\sqrt{3}\dot{\gamma}\tau/12)^{1/3}} \right) + \left[ \frac{C e^{-\Delta \tilde{U}_{\pi/6}(\Delta \Theta)}}{1 + C e^{-\Delta \tilde{U}_{\pi/6}(\Delta \Theta)}} \right] \times \text{Erfc} \left( \frac{(\sqrt{3}\dot{\epsilon}\tau/2 + 7\dot{\gamma}\tau^*/6)^{1/3}}{(\sqrt{3}\dot{\epsilon}\tau/2 + 7\dot{\gamma}\tau/6)^{1/3}} \right) \quad (\text{A19})$$

for both  $\Theta_0 = \pi/6$  and  $\Theta_0 = \pi/3$ .

### ACKNOWLEDGMENTS

This research was supported in part by the National Science Foundation through TeraGrid resources under Grant No. TG-DMR090139. We also thank the National Defense Science and Engineering Fellowship and NSF CAREER Award No. 1054671 for financial support.

<sup>1</sup>P. G. de Gennes, *J. Chem. Phys.* **60**, 5030 (1974).

<sup>2</sup>S. Liu, B. Ashok, and M. Muthukumar, *Polymer* **45**, 1383 (2004).

<sup>3</sup>I. M. Neelov, D. B. Adolf, A. V. Lyulin, and G. R. Davies, *J. Chem. Phys.* **117**, 4030 (2002).

<sup>4</sup>A. Buguin and F. Brochard-Wyart, *Macromolecules* **29**, 4937 (1996).

<sup>5</sup>R. G. Larson, *J. Rheol.* **49**, 1 (2005).

<sup>6</sup>D. Smith, H. Babcock, and S. Chu, *Science* **1724** (1999).

<sup>7</sup>T. T. Perkins, D. E. Smith, and S. Chu, *Science* **276**, 2016 (1997).

- <sup>8</sup>J. S. Hur, E. S. G. Shaqfeh, and R. G. Larson, *J. Rheol.* **44**, 713 (2000).
- <sup>9</sup>R. M. Jendrejack, J. J. de Pablo, and M. D. Graham, *J. Chem. Phys.* **116**, 7752 (2002).
- <sup>10</sup>J. M. Kim and P. S. Doyle, *Lab Chip* **7**, 213 (2007).
- <sup>11</sup>J. M. Kim and P. S. Doyle, *J. Chem. Phys.* **125**, 074906 (2006).
- <sup>12</sup>A. Alexander-Katz, M. F. Schneider, S. W. Schneider, A. Wixforth, and R. R. Netz, *Phys. Rev. Lett.* **97**, 138101 (2006).
- <sup>13</sup>A. Alexander-Katz and R. R. Netz, *Macromolecules* **41**, 3363 (2008).
- <sup>14</sup>A. Alexander-Katz and R. R. Netz, *EPL* **80**, 18001 (2007).
- <sup>15</sup>S. W. Schneider, S. Nuschele, A. Wixforth, C. Gorzelanny, A. Alexander-Katz, R. R. Netz, and M. F. Schneider, *Proc. Natl. Acad. Sci. U.S.A.* **104**, 7899 (2007).
- <sup>16</sup>C. E. Sing and A. Alexander-Katz, *Macromolecules* **43**, 3532 (2010).
- <sup>17</sup>N. Hoda and S. Kumar, *J. Chem. Phys.* **16**, 164907 (2008).
- <sup>18</sup>S. Goto, D. R. Salomon, Y. Ikeda, and Z. M. Ruggeri, *J. Biol. Chem.* **270**, 23352 (1995).
- <sup>19</sup>W. S. Nesbitt, E. Westein, F. J. Tovar-Lopez, E. Tolouei, A. Mitchell, J. Fu, J. Carberry, A. Fouras, and S. P. Jackson, *Nat. Med.* **15**, 665–U146 (2009).
- <sup>20</sup>P. Szymczak and M. Cieplak, *J. Chem. Phys.* **127**, 155106 (2007).
- <sup>21</sup>J. Rotne and S. Prager, *J. Chem. Phys.* **50**, 4831 (1969).
- <sup>22</sup>H. Yamakawa, *J. Chem. Phys.* **53**, 436 (2003).
- <sup>23</sup>N. J. Woo and E. S. G. Shaqfeh, *J. Chem. Phys.* **119**, 2908 (2003).
- <sup>24</sup>B. D. Hoffman and E. S. G. Shaqfeh, *J. Rheol.* **51**, 947 (2007).
- <sup>25</sup>R. G. Larson and J. J. Magda, *Macromolecules* **22**, 3004 (1989).
- <sup>26</sup>Z. M. Ruggeri and G. L. Mendolicchio, *Circ. Res.* **100**, 1673 (2007).
- <sup>27</sup>H. Chen and A. Alexander-Katz, *Biophys. J.* **100**, 174 (2011).
- <sup>28</sup>X. Zhang, K. Halvorsen, C.-Z. Zhang, W. P. Wong, and T. A. Springer, *Science* **324**, 1330 (2009).
- <sup>29</sup>C. E. Sing and A. Alexander-Katz, *Biophys. J.* **98**, L35 (2010).
- <sup>30</sup>M. Doi and S. Edwards, *The Theory of Polymer Dynamics* (Oxford University Press, New York, 1986).